OXFORD

ORIGINAL ARTICLE

Functional Connectivity Predicts Individual Development of Inhibitory Control during Adolescence

Haiyan Wang[1,2], Lingzhong Fan[1,2], Ming Song[1], Bing Liu[1,2,3], Dongya Wu[1,2], Rongtao Jiang[1,2], Jin Li[1], Ang Li[1,2], Tobias Banaschewski[4], Arun L.W. Bokde[5], Erin Burke Quinlan[6], Sylvane Desrivières[6], Herta Flor[7,8], Antoine Grigis[9], Hugh Garavan[10], Bader Chaarani[10], Penny Gowland[11], Andreas Heinz[12], Bernd Ittermann[13], Jean-Luc Martinot[14], Marie-Laure Paillère Martinot[15], Eric Artiges[16], Frauke Nees[4,7], Dimitri Papadopoulos Orfanos[9], Luise Poustka[17], Sabina Millenet[4], Juliane H. Fröhner[18], Michael N. Smolka[18], Henrik Walter[12], Robert Whelan[19], Gunter Schumann[6,20,21,22,*] and Tianzi Jiang[1,2,3,23,24,*]

[1]Brainnetome Center and National Laboratory of Pattern Recognition, Institute of Automation, Chinese Academy of Sciences, Beijing 100190, China, [2]School of Artificial Intelligence, University of Chinese Academy of Sciences, Beijing 100049, China, [3]CAS Center for Excellence in Brain Science and Intelligence Technology, Institute of Automation, Chinese Academy of Sciences, Beijing 100190, China, [4]Department of Child and Adolescent Psychiatry and Psychotherapy, Central Institute of Mental Health, Medical Faculty Mannheim, Heidelberg University, 68159 Mannheim, Germany, [5]Discipline of Psychiatry, School of Medicine and Trinity College Institute of Neuroscience, Trinity College Dublin, Dublin 2, Ireland, [6]Centre for Population Neuroscience and Precision Medicine (PONS), Institute of Psychiatry, Psychology & Neuroscience, SGDP Centre, King's College London, London SE5 8AF, United Kingdom, [7]Institute of Cognitive and Clinical Neuroscience, Central Institute of Mental Health, Medical Faculty Mannheim, Heidelberg University, 68159 Mannheim, Germany, [8]Department of Psychology, School of Social Sciences, University of Mannheim, 68131 Mannheim, Germany, [9]NeuroSpin, CEA, Université Paris-Saclay, F-91191 Gif-sur-Yvette, France, [10]Departments of Psychiatry and Psychology, University of Vermont, 05405 Burlington, VT, USA, [11]Sir Peter Mansfield Imaging Centre School of Physics and Astronomy, University of Nottingham, University Park, Nottingham, NG7 2RD, United Kingdom, [12]Department of Psychiatry and Psychotherapy CCM, Charité - Universitätsmedizin Berlin, Charitéplatz 1, 10117, Berlin, Germany, [13]Physikalisch-Technische Bundesanstalt (PTB), Braunschweig and Berlin, 10587 Berlin, Germany, [14]Institut National de la Santé et de la Recherche Médicale, INSERM Unit 1000 "Neuroimaging & Psychiatry", University Paris Sud—University Paris Saclay, DIGITEO Labs, Rue Noetzlin, 91190 Gif sur Yvette, France, [15]Institut National de la Santé et de la Recherche Médicale, INSERM Unit 1000 "Neuroimaging & Psychiatry", University Paris Sud, University Paris Descartes; and AP-HP.Sorbonne Université, Department of Child and Adolescent Psychiatry, Pitié-Salpêtrière Hospital, 75013, Paris, France, [16]Institut National de la Santé et de la Recherche Médicale, INSERM Unit 1000 "Neuroimaging & Psychiatry",

University Paris Sud—University Paris Saclay, DIGITEO Labs, Gif sur Yvette; and Psychiatry Department 91G16, Orsay Hospital, Orsay, France, [17]Department of Child and Adolescent Psychiatry and Psychotherapy, University Medical Centre Göttingen, 37075 Göttingen, Germany, [18]Department of Psychiatry and Neuroimaging Center, Technische Universität Dresden, Chemnitzer Str. 46a01187, Dresden, Germany, [19]School of Psychology and Global Brain Health Institute, Trinity College Dublin, Dublin 2, Ireland, [20]PONS Research Group, Department of Psychiatry and Psychotherapy, Campus Charite Mitte, Humboldt University, 10117 Berlin, Germany, [21]Leibniz Institute for Neurobiology, 39118 Magdeburg, Germany, [22]Institute for Science and Technology of Brain-inspired Intelligence (ISTBI), Fudan University, Shanghai 200433, China, [23]The Clinical Hospital of Chengdu Brain Science Institute, MOE Key Lab for Neuroinformation, University of Electronic Science and Technology of China, Chengdu 625014, China and [24]The Queensland Brain Institute, University of Queensland, Brisbane, Queensland 4072, Australia

*Address correspondence to Tianzi Jiang, Brainnetome Center, Institute of Automation, Chinese Academy of Sciences, Beijing 100190, China. Email: jiangtz@nlpr.ia.ac.cn; Gunter Schumann, Centre for Population Neuroscience and Stratified Medicine, Institute of Psychiatry, Psychology and Neuroscience, MRC-SGDP Centre, King's College London, 16 De Crespigny Park, London SE5 8AF, United Kingdom. Email: gunter.schumann@kcl.ac.uk.

Abstract

Derailment of inhibitory control (IC) underlies numerous psychiatric and behavioral disorders, many of which emerge during adolescence. Identifying reliable predictive biomarkers that place the adolescents at elevated risk for future IC deficits can help guide early interventions, yet the scarcity of longitudinal research has hindered the progress. Here, using a large-scale longitudinal dataset in which the same subjects performed a stop signal task during functional magnetic resonance imaging at ages 14 and 19, we tracked their IC development individually and tried to find the brain features predicting their development by constructing prediction models using 14-year-olds' functional connections within a network or between a pair of networks. The participants had distinct between-subject trajectories in their IC development. Of the candidate connections used for prediction, ventral attention-subcortical network interconnections could predict the individual development of IC and formed a prediction model that generalized to previously unseen individuals. Furthermore, we found that connectivity between these two networks was related to substance abuse problems, an IC-deficit related problematic behavior, within 5 years. Our study reveals individual differences in IC development from mid- to late-adolescence and highlights the importance of ventral attention-subcortical network interconnections in predicting future IC development and substance abuse in adolescents.

Key words: adolescence, functional connectivity, inhibitory control, longitudinal prediction, stop signal task

Introduction

Inhibitory control (IC), the ability to stop unwanted or inappropriate actions and thoughts in a timely manner, underlies the performance of goal-directed behaviors. Derailment of IC is considered integral to numerous psychiatric and behavioral disorders (Verbruggen and Logan 2008). Given the fact that many of these disorders emerge during adolescence (Paus et al. 2008), they are considered to be neurodevelopment disorders and relate to abnormal development (Insel 2014). Adolescents are a heterogeneous group, with striking individual differences in both behavioral and neural developments (Foulkes and Blakemore 2018). Studying the development of IC during adolescence at the individual level and finding the early neural predictors of its future development can help identify adolescents at risk of IC deficits and provide neural evidence for early and targeted interventions.

Many researchers have studied the development of IC in adolescence, but the results were inconsistent and fell broadly into the three different development patterns proposed by Casey (2015). Specifically, some studies suggest a steady increase of IC from childhood to adulthood (Velanova et al. 2008; Aite et al. 2018), some studies imply a decelerated or stopped

improvement in IC from adolescence to adulthood (Luna et al. 2004; Ordaz et al. 2013; Humphrey and Dumontheil 2016), whereas some studies revealed that IC improved until adolescence, and then diminished slightly in young adults (Schachar and Logan 1990; Williams et al. 1999). Due to the discordance of these results derived from commonly used group-level analyses, we hypothesized that IC may show different developmental trajectories in different adolescents. Large-scale longitudinal datasets investigating potential individual differences are required to advance this field (Foulkes and Blakemore 2018). Of the limited number of longitudinal studies of IC development during adolescence, one study showed significant individual differences in the development of IC from early- to midadolescence (Fosco et al. 2019). Nonetheless, it is unclear whether there are individual variations in the development of IC from mid- to late-adolescence, the period with the highest level of sensation seeking (Steinberg et al. 2018).

Previous investigations of the neural mechanisms underlying IC development primarily focused on finding age-related changes in brain activation during IC-related tasks (Durston et al. 2002; Rubia et al. 2007; Paulsen et al. 2015) and in the brain connectivity underlying IC (Liston et al. 2006; Hwang et al.

2010; Vink et al. 2014). Although this kind of approach has discovered the brain systems showing developmental changes associated with IC development, it may be more beneficial to predict the individual future development of IC using current brain features. This could enable us to find neural predictors and potential intervention targets associated with IC development and might be especially relevant for adolescents, as adolescence is a developmental period characterized by mental and physical health vulnerability, but also opportunities for interventions (Rosenberg et al. 2018). Nevertheless, the scarcity of longitudinal data has hindered the progress of such a predictive study.

IC-related functional connectivity derived from task functional magnetic resonance imaging (fMRI) correlates with individual differences in IC (Tsvetanov et al. 2018), and many of these connections show a protracted development until early adulthood (Hwang et al. 2010; Vink et al. 2014). Moreover, compared with functional connectivity during resting-state, cognitive tasks could amplify trait-relevant individual differences in patterns of functional connectivity (Greene et al. 2018). These previous findings suggest the potential usefulness of task-related functional connectivity for predicting individual IC development.

Substance abuse is an IC-deficit related maladaptive behavior, and problems in IC during adolescence are considered to be a risk factor for the development of substance abuse (Romer Thomsen et al. 2018). Experiment with substances and onset of substance abuse primarily concentrate in adolescence (Chambers et al. 2003), which has long-lasting detrimental effects on the developing brain (O'Shea et al. 2004). Altered IC-related functional connections have been found in substance abusers (Filbey and Yezhuvath 2013; Akkermans et al. 2018), but it is not known whether these alterations precede substance abuse.

To analyze the developmental trajectory of IC from mid- to late-adolescence and discover the brain features predicting its future development, we employed the longitudinal IMAGEN dataset (Schumann et al. 2010), in which subjects performed a stop signal task (SST) during fMRI scanning at both 14 (baseline) and 19 years old (follow-up). SST requires subjects to cancel an already initiated motor response (Logan and Cowan 1984), and the time required for the cancelation process (stop signal reaction time, SSRT) has been demonstrated to be a reliable index of IC (Congdon et al. 2012). We first examined the development trajectory of SSRT from baseline to follow-up at the individual level. Then, using a cross-validated, data-driven approach, we sought to identify the brain features predicting the development measured by the SSRT using the baseline functional connectivity after regressing out the effect of nuisance covariates and the baseline SSRT ($N = 326$, subjects with baseline fMRI, baseline SSRT, and follow-up SSRT). To test the generalizability of the prediction model, we further tested it on a previously unseen cohort ($N = 344$, subjects with baseline fMRI and follow-up SSRT, but without baseline SSRT). In addition, we examined whether the brain features predicting SSRT development were also associated with future substance abuse, an IC-deficit related problematic behavior ($N = 158$).

Materials and Methods

Participants

Data for this work came from the multisite longitudinal IMAGEN project (Schumann et al. 2010), in which over 2000 adolescents of about age 14 were recruited from schools in France, the UK, Ireland, and Germany. Behavioral, cognitive, and neuroimaging data were acquired, and the participants were followed longitudinally. This study received ethical approval from each local ethics research committee. Written consent was obtained from the participants' guardian, and verbal assent was obtained from each adolescent. A more detailed description can be found in the standard operating procedures for the IMAGEN project (https://imagen-europe.com/resources/standard-operating-procedures/). Here, data from age 14 (baseline) and 19 (follow-up) were used. We only included subjects who had complete demographic information, including age, gender, handedness, acquisition site, verbal IQ, and performance IQ.

IQ was determined using the Wechsler Intelligence Scale for children at only the baseline. This scale includes the following subscales: blocks design, digit span, matrix reasoning, vocabulary, and similarities. Performance IQ was determined by summing the raw scores of the block design, digit span, and matrix reasoning subscales. The total score of the vocabulary and similarities subscales was used to evaluate verbal IQ.

Stop Signal Task

SST is an important tool for studying IC (Verbruggen and Logan 2008). There were 1821 and 1306 subjects who participated in an SST at the baseline and follow-up, respectively. The SST in this study consisted of 400 go trials intermingled with 80 stop trials at the baseline and 300 go trials mixed with 60 stop trials at the follow-up. In the go trials, the volunteers were required to respond to regularly presented visual go stimuli (arrows pointing left or right shown for 1000 ms) with a button-press, whereas in the stop trials they had to try to suppress their motor response when the go stimulus was followed unpredictably by a stop stimulus (an arrow pointing upwards shown for 100–300 ms). Successive stop trials occurred randomly between 3 and 7 go trials. The intertrial interval was jittered between 1.6 s and 2 s to enhance statistical efficiency (Dale 1999). In addition, if the subject responded to the go stimulus before the stop stimulus presentation (Stop Too Early, STE), this stop trial was repeated, but only the first 7 STEs were repeated.

Stopping difficulty was manipulated with a tracking algorithm by varying the stop signal delay (SSD, the time interval between the onset of the go stimulus and that of the stop stimulus, 50 ms steps, initial SSD = 150 ms) based on each participant's performance. This produced about 50% accuracy on stop trials for each subject. There was a subtle difference in the tracking algorithms of the baseline and follow-up, with the SSD in each stop trial adjusted according to all the previous stop trials in the baseline (percentage of successful stop trials, recalculated after each stop trial), but this was adjusted according to the success or failure of the immediately previous stop trial in the follow-up. During the subsequent SSRT analysis, we only included subjects in which the tracking algorithms worked well in manipulating the stopping difficulty, i.e., the percentage of accuracy on the stop trials was 40–60%.

SSRT Analysis

In the SST, the time taken to cancel the imminent go response (SSRT), which was calculated from the SST response outcomes, including Go Success, Go Wrong, Go Too Late, Stop Success, Stop Failure, and STE, is an important measure of IC. A low SSRT represents good IC. The estimation method for the SSRT at both the baseline and the follow-up was in line with previous

studies utilizing these data (Whelan et al. 2012; White et al. 2014). Specifically, we first excluded subjects who had more than 20% errors (Go Wrong or Go Too Late) on the go trials. Also, since the STE trials would affect the estimation of the SSRT, the SSRT was calculated up to the eighth STE for participants who had more than 8 STEs. Since this occurred early in some subjects, the SSRT estimation was restricted to subjects who did not reach the eighth STE before their 300th trial. In addition, the SSRT was estimated based on the independent horse-race model, which assumes an independent race between the go and stop processes. If the independent race assumption is violated, the SSRT estimation becomes unreliable. The independent horse-race assumption was tested by comparing the mean reaction time (RT) on unsuccessful stop trials against the mean RT on go trials for each subject. As suggested in a consensus guide on SST (Verbruggen et al. 2019), the SSRT analysis was not performed when the RT on unsuccessful stop trials was numerically longer than the RT on go trials.

SSRT was computed using the integration method, which has been shown to be less susceptible than the frequently used mean method to the shape of the RT distribution (Verbruggen et al. 2013). Specifically, we estimated the SSRT by subtracting the mean SSD from the Go Success RT at the percentile corresponding to the proportion of Stop Failure trials (pSF). pSF was calculated as the ratio of Stop Failure trials in the valid stop trials (Stop Success and Stop Failure trials). We did not include STE trials when calculating the pSF as the STEs included in the SSRT analysis were repeated by a new stop trial. Of all the subjects who performed the SST, 805 individuals at the baseline and 1053 individuals at the follow-up met the criteria for estimating SSRT. Also, SSRTs below 80 were excluded (1 subjects in baseline, 4 subjects in follow-up) (Cohen et al. 2010), generating 804 and 1049 valid SSRTs ($N = 458$ in common) at the baseline and follow-up, respectively.

Threshold for a Reliable SSRT Change

To quantify the SSRT-related development, we defined ΔSSRT as baseline SSRT minus follow-up SSRT so that a positive ΔSSRT denotes an improvement in IC from baseline to follow-up. To further determine whether each individual ΔSSRT was statistically significant, we defined a threshold for significant ΔSSRTs based on the reliable change index (RCI). The RCI can be calculated by dividing ΔSSRT by the standard error of the difference (S_{diff}), which is related to the standard deviation and reliability of the SSRT measure (Iverson 2001), yielding a pseudo-z-statistic. To assess the reliability of the SSRT measure, we used split-half reliability with Spearman-Brown correction (Zahra and Hedge 2010). Specifically, for each subject, we randomly split the go and stop trials used in the SSRT calculation into 2 halves and recalculated the SSRT based on the 2 halves (Congdon et al. 2012). Then we calculated the Pearson's correlation coefficient of the SSRTs between the 2 halves across the subjects. This process was repeated 100 times, and the median of the 100 correlation coefficients was referred to as the final split-half reliability. One problem with split-half reliability is that the reliability is underestimated since only half of the trials are used. To get a better estimate of the reliability of the full set, we applied the Spearman–Brown correction, which has been shown to provide a good estimate of what the reliability coefficient would be if the halves were increased to the original length (Kelley 1925). The correction formula is $r_{ii} = 2r_{hh}/(1 + r_{hh})$, where r_{hh} is the split-half correlation coefficient, and r_{ii} represents the corrected value.

As the RCI is a pseudo-z-statistic, which approximately follows the standard normal distribution, absolute RCIs larger than 1.96 were treated as significant changes beyond the two-tailed 95% confidence interval (Plitt et al. 2015). Finally, the significant ΔSSRT threshold was formed by multiplying the S_{diff} by 1.96.

Image Acquisition and Preprocessing

Event-related fMRI data were acquired while the participants were performing the SST. The subjects were familiarized with the task by performing a practice session of 60 trials outside the scanner. In this study, the SST-related fMRI at baseline was used. Specifically, fMRI data were collected at 8 sites on 3 T MRI systems made by 4 manufacturers (Siemens, Philips, General Electric, and Bruker). The scanning parameters and sequence protocol were specifically chosen to be compatible with all scanners to ensure comparison of the fMRI data from the different sites. Nevertheless, the effect of site was controlled by adding it as a nuisance covariate in our analyses. Standardized hardware for visual stimulus presentation (Nordic Neurolab, Bergen, Norway) was used at all sites. The functional runs included 444 whole-brain volumes acquired for each participant using a gradient-echo, echo-planar imaging (EPI) sequence. Each volume contained 40 axial slices aligned to the anterior commissure–posterior commissure line (2.4 mm slice thickness, 1 mm gap). The echo time was optimized (echo time = 30 ms, repetition time = 2200 ms) to provide reliable imaging of subcortical areas. The flip angle was 75° and the in-plane resolution was 3.4 × 3.4 mm with a field of view of 220 × 220 mm.

The fMRI data were first manually checked for quality and subjects with a lack (mainly in the superior parietal and inferior temporal lobes) of whole-cerebrum coverage were removed. We also excluded subjects who had excessive head motion (defined a priori as >3 mm translation or >3° rotation) during the fMRI acquisition. The preprocessing of fMRI data was done with SPM8 (Statistical Parametric Mapping, https://www.fil.ion.ucl.ac.uk/spm/) and custom scripts. Time-series data were corrected for slice-timing and movement and then nonlinearly warped into MNI space using a custom EPI template (53 × 63 × 46 voxels). The voxels were resampled to a resolution of 3 × 3 × 3 mm. In addition, linear drift, head motion parameters (3 rotations and 3 translations), and mean signal from the cerebrospinal fluid, white matter, and the whole brain were regressed out of the data. Then, high-pass filtering (0.01 Hz) was performed (Kaufmann et al. 2017; Beaty et al. 2018), and the data were smoothed with a 5-mm full width half maximum Gaussian kernel. Finally, we performed "scrubbing" to remove scans in which the framewise displacement (FD) were > 0.5 mm (Power et al. 2012). To ensure enough volumes for further fMRI analyses, we excluded subjects who had fewer than half of their volumes remaining after the scrubbing.

Functional Connectivity Measures and Feature Matrices

Brain nodes in the functional connectivity calculation were defined using Power's atlas (Power et al. 2011), which has 264 spherical regions of interest (ROIs) with a radius of 5 mm. Here we chose Power's atlas because it provides definitions of cortical and subcortical ROIs as well as networks, which enabled us to directly categorize ROIs into networks. Moreover, the brain activations during IC-related tasks have been shown to be mainly distributed in the salience, frontoparietal (FPN), ventral attentional (VAN) and default mode networks (DMN) (Cai et al. 2019),

and all of these networks are well established in Power's atlas. Among the 264 ROIs, we excluded the 28 ROIs without a defined network and the 4 ROIs located in the cerebellum, which was not fully covered in some subjects. The time series of the fMRI were extracted and averaged across voxels within each of the remaining 232 ROIs. For each subject, the Pearson's correlation coefficients between the time series of each possible pair of ROIs were calculated and used to construct a 232×232 symmetrical functional connectivity matrix, which was then Fisher z-transformed.

Each of the 232 ROIs belongs to one of 12 networks, including sensory/somatomotor hand (SM_H), sensory/somatomotor mouth (SM_M), cingulo-opercular task control (Cing_Oper), auditory, DMN, memory retrieval (Memory), visual, FPN, salience, subcortical, VAN, and dorsal attention (DAN) networks (Power et al. 2011). Based on these networks, connections in the functional connectivity matrix were divided into 78 groups: 12 within-network connectivity groups and 66 ($12 \times 11/2$) between-network connectivity groups (Fig. 1A). Using each connectivity group, we constructed a $N_s \times N_f$ feature matrix, where N_s is the number of subjects and N_f denotes the number of features, that is, the number of connections in each within-network ($N \times (N-1)/2$, where N denotes the number of ROIs in this network) or between-network ($N_i \times N_j$, where N_i and N_j are the number of ROIs in network i and network j, respectively) connectivity group. Here both within-network and between-network connections were used as features, because both of them were found to contribute to predicting brain maturity (Dosenbach et al. 2010). Specifically, the functional maturation of brain is driven by the segregation of regions close in anatomical space, and the integration of distant regions into functional networks (Fair et al. 2009). In addition to within-network connections, between-network connections were also found to be associated with IC (Tsvetanov et al. 2018), and other cognitive abilities (Rosenberg et al. 2016; Beaty et al. 2018; Yamashita et al. 2018) as well as future changes of clinical symptoms (Plitt et al. 2015).

Prediction of SSRT Development Using Baseline Functional Connectivity

Subjects who had valid data for the baseline and follow-up SSRT as well as a baseline SST-related fMRI were included in the SSRT development prediction analyses ($N = 326$). To eliminate the potential effects of demographic factors on prediction, we regressed out the site information (the only demographic information affecting ΔSSRT in our dataset, see Results) and baseline SSRT from the ΔSSRT. The ΔSSRT residual was further used as the index to be predicted. This process, similar to a hierarchical regression, allowed us to discover how well the brain features could predict the development of SSRT after factoring out the effects of nonbrain information (Plitt et al. 2015).

We built 78 prediction models to predict the ΔSSRT residual using each of the 78 feature matrices defined above (Fig. 1B). For each functional connectivity feature matrix, we implemented a partial least squares regression analysis to model their relationship to the ΔSSRT residual, using the plsregress function in Matlab. To reduce the effect of overfitting, we employed a 10-fold cross-validation (CV) strategy, which was carried out with our custom Matlab scripts. Specifically, we first randomly divided the full dataset into 10 subsets, and then each subset was iteratively used as the test set, whereas the other 9 subsets were used as the training set. Since the performance could depend on data division, the 10-fold CV was repeated 100 times. Correlation coefficients (r) between the predicted and actual ΔSSRT residual were calculated and the median of the r values across the 100 repetitions was referred to as the prediction performance. Given that head motion and the number of frames retained after scrubbing can confound functional connectivity analyses (Gordon et al. 2017), we controlled for baseline FD as well as the number of remaining frames when calculating r.

The significance of the prediction performance was determined using a permutation test. Specifically, we reran the prediction process using the same data but shuffled the observed ΔSSRT residual. The pairing of functional connectivity features and fMRI confounding factors (baseline FD and the number of remaining frames) was preserved (Yamashita et al. 2018). By repeating this process 10 000 times, we generated a null distribution of r values. The corresponding P value was computed using the following formula: (1 + the number of permuted r values greater than or equal to the empirical r)/(1 + the number of permutation times). Since there were 78 models in total, the Bonferroni correction for multiple comparisons was used ($P = 0.05/78 = 6.41 \times 10^{-4}$).

For the prediction model whose performance survived the Bonferroni correction, we utilized the method proposed in a previous study (Yoo et al. 2017) to find connections with statistically significant weights in the model. Practically, we reconstructed the partial least squares regression model using all the 326 subjects. The same permutation test was performed as that in determining the significance of the prediction performance. The beta coefficients in the regression for every edge were obtained from each permutation, and significance for each edge was determined by whether its real beta value differed (two-tailed $P < 0.05$) from the empirical distribution acquired from the 10 000 permutations.

Effects of Choosing Different Functional Connectivity Metrics on the Prediction Model

In addition to the Pearson's correlation coefficients, we used another 2 functional connectivity measures (accordance and discordance) to examine the effects of different functional connectivity metrics on the prediction model. The accordance and discordance were proposed to respectively track in-phase synchronization and out-of-phase anticorrelation (Meskaldji et al. 2015), and have been used to predict individual attention ability (Yoo et al. 2017). To calculate accordance and discordance, the mean time-series of each ROI were first thresholded with a predefined quantile of q to retain only significant signals and exclude noise. This q-value means that only $(1-q) \times 100\%$ of the lowest (deactivations) and highest (activations) signals in the time series would remain. In our study, the q-value was chosen from 70 to 90 with a step of 5. Accordance between each pair of time-series measures the degree to which they are coactivated and codeactivated. Specifically, it was calculated as the size of the union of coactivated and codeactivated time points, and then normalized by the size of the union of significant activated and deactivated time points of the 2 time-series. Similarly, discordance measures the degree to which 2 signals are oppositely activated or deactivated, and was calculated as the normalized size of activated–deactivated and deactivated–activated extreme time points of the 2 signals.
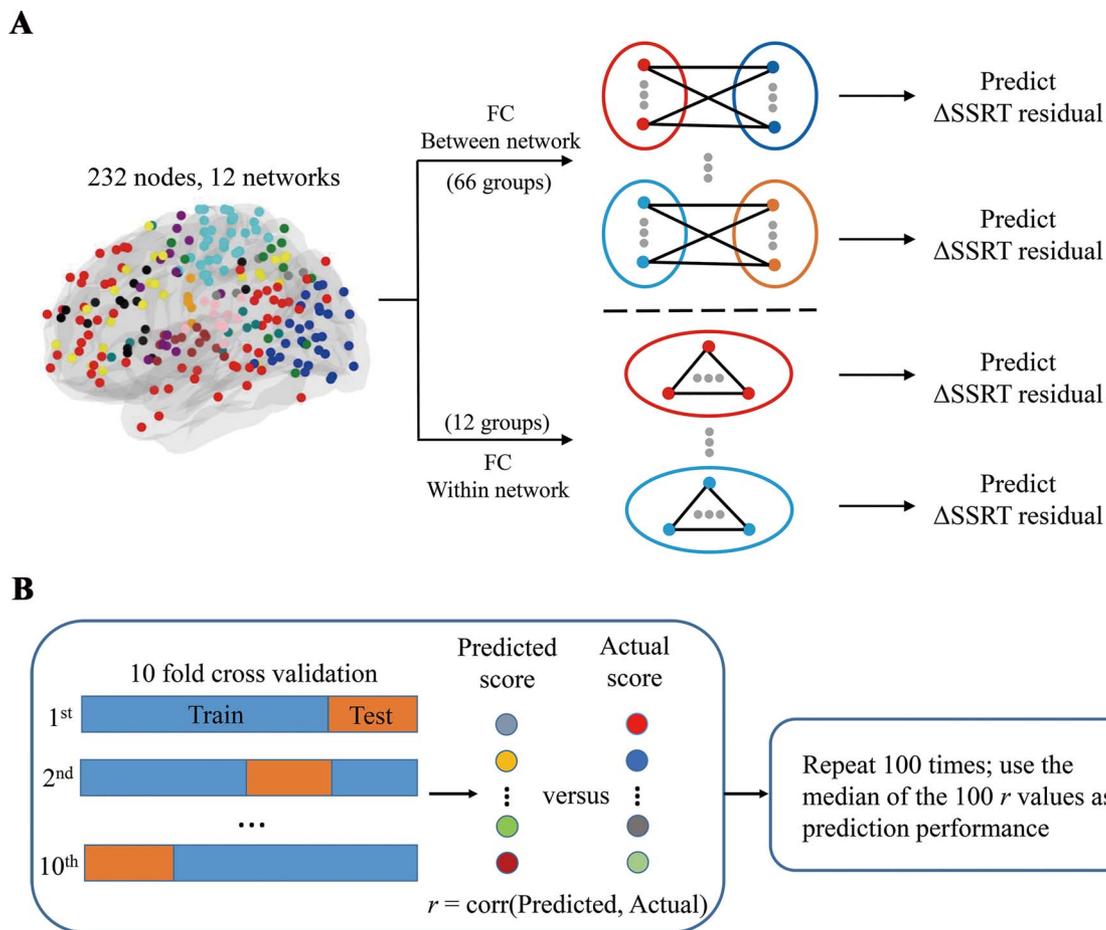
Figure 1. Flowchart of ΔSSRT residual prediction using brain functional connectivity profiles. (A) Definition of functional connectivity features. Brain nodes were defined by a predefined atlas with each node belonging to 1 of the 12 networks. Functional connections for each possible pair of ROIs between 2 networks or within 1 network were calculated, generating 66 groups of between-network and 12 groups of within-network connections. Each group of connections was separately used to predict the ΔSSRT residual. (B) The 10-fold CV prediction process. For each group of connectivity features, a partial least squares regression analysis was used to learn their relationship with the ΔSSRT residual. 10-fold CV was used to avoid overfitting; this was repeated 100 times to reduce the effect of data division. The median of the 100 *r* values and its corresponding *P* value (derived from 10 000 random permutations) was used to evaluate the prediction performance of each model.

Relationship with Future Substance Abuse

The participants completed questionnaires about their substance use behaviors (alcohol, nicotine, and illicit drugs) at both the baseline and follow-up. In our work, we employed questionnaires including the European School Survey Project on Alcohol and Drugs (ESPAD) (Hibell et al. 1997), the Fagerstrom Test for Nicotine Dependence (FTND) (Heatherton et al. 1991), and the Alcohol Use Disorders Identification Test (AUDIT) (Saunders et al. 1993). The ESPAD reports alcohol, nicotine, and illicit drugs use frequency during the 30 days immediately prior to the survey as well as during the lifetime. AUDIT is a 10-item questionnaire covering the domains of alcohol consumption, drinking behavior, and alcohol-related problems, with a total AUDIT score greater than 7 denoting alcohol dependent. Participants who reported "1-5 cigarettes per day" or more during the last 30 days on ESPAD further finished the FTND questionnaire, which is a 6-item questionnaire for assessing nicotine dependence symptoms (the summed FTND score: 0 points = "not dependent", 1–3 points = "less dependent", 4–6 points = "moderately dependent", 7–10 points = "highly dependent"). For illicit drugs, problem use thresholds for each kind of drug were determined based on a previous study

utilizing these data (≥ 40 lifetime use occasions for hash; ≥ 3–5 occasions for glue, tranquilizers, amphetamine, lysergic acid diethylamide, hallucinogenic mushrooms, ecstasy, ketamine, and liquid ecstasy; ≥ 1–2 occasions for crack, cocaine, heroin, narcotics, and anabolic steroids) ((Büchel et al. 2017).

According to the above questionnaires, substance nonusers were defined as subjects with no alcohol or nicotine use during the last 30 days and no lifetime illicit drug use, and substance abusers were defined as subjects who abused any of the substances. To test whether the functional connectivity features that could predict SSRT-related development were associated with future substance abuse, we identified the future substance abuse group (subjects who are substance nonusers at baseline but became substance abusers at follow-up) and the control group (subjects who were substance nonusers at both baseline and follow-up). The functional connections between each pair of networks were summed as a brain measure for each subject at the baseline. An analysis of covariance (ANCOVA) was used to compare the baseline brain measures between the 2 groups, controlling for the effect of demographic information (baseline age, age latency, gender, handedness, site, verbal IQ, performance IQ) as well as the baseline fMRI confounding factors (FD and the

number of remaining frames). The ANCOVA was conducted with the anovan function in Matlab.

It should be noted that, to reduce the effect of substance use on the baseline brain, both groups were substance nonusers at baseline. However, compared with illicit drugs, alcohol, or nicotine nonusers were defined as subjects with no alcohol or nicotine use during the 30 days immediately prior to the survey, instead of during the lifetime span. We did this because no alcohol or nicotine use during the lifetime span will result in too small a sample size ($N = 13$ for the control group) in our study and thus reduce the statistical power. However, this would introduce differences in the lifetime alcohol or nicotine use by baseline between the two groups. In addition, the age of the first experiment with substances would also affect later substance abuse (Sinha et al. 2003). So, in addition to covariates mentioned above, we regressed out the lifetime use and time-to-initiation of alcohol and nicotine at baseline in the ANCOVA. For subjects who have not initiated any substance, we used a relatively older age, i.e., 20 years old (40, 60, and 80 years old were also tried), to represent their time-to-initiation.

The significance of the difference for the ANCOVA was derived from a permutation test in which we randomly shuffled the group labels and reran the ANCOVA (10 000 times). The baseline SSRTs and ∆SSRTs between the future substance abuse group and the control group were also compared using ANCOVAs, controlling the same covariates except for the baseline fMRI confounding factors.

Results

Individual Differences in SSRT-Measured IC Development

We began by analyzing the longitudinal development measured by the SSRT of the 326 subjects from baseline to follow-up. Detailed demographic information and SST performance for these participants are shown in Table 1. To ensure the comparability of the SSRT between baseline and follow-up, we employed identical screening criteria and the same integration estimation method for the SSRT at baseline and follow-up. The reliability (split-half reliability with Spearman–Brown correction) of the SSRT measure at baseline and follow-up was 0.84 and 0.95, respectively, which showed good (excellent) reliability of SSRT at baseline (follow-up) (<0.57 is poor, 0.57–0.74 is fair, 0.75–0.85 is good, and 0.86–1 is excellent). The interpretation of reliability was in accordance with the criteria used in a previous study (Congdon et al. 2012). Since the criteria was for split-half reliability, we adapted it using a Spearman–Brown correction.

On average, there was a significant increase in the SSRT (two-tailed paired t-test, $t_{325} = -3.09$, $P = 0.002$) from baseline to follow-up, indicating a decline in IC at the group level. To quantify the development measured by the SSRT, we defined ∆SSRT as baseline SSRT minus follow-up SSRT, so that a positive ∆SSRT indicated an improvement in IC. To further examine whether each individual's change in SSRT from baseline to follow-up was significant or caused by estimation error, we derived a threshold of 31.88 ms for a true change in SSRT based on the RCI. Put differently, ∆SSRTs whose absolute values were longer than 31.88 ms were treated as significant changes beyond the two-tailed 95% confidence interval. According to this threshold, the development measured by the SSRT from baseline to follow-up showed different developmental trajectories across individuals (Fig. 2A). The proportion of subjects who showed a significantly

decreased or increased SSRT were 17.48% and 29.45%, respectively, whereas 53.07% of subjects did not show a significant SSRT change from baseline to follow-up. Moreover, without considering the baseline SST-related fMRI data during the data screening, 458 subjects with both baseline and follow-up SSRTs were obtained, and the proportion of decreased/stable/increased SSRT was 16.81%, 53.06%, and 30.13%, respectively (Table S1 and Fig. S1).

Demographic Effects on SSRT Development

We next examined the effect of each demographic category (including baseline age, age latency, gender, handedness, acquisition site, baseline verbal IQ, and baseline performance IQ) on ∆SSRT (Table S2). Only site had a significant effect on ∆SSRT (one-way ANOVA, $F_{7,318} = 2.09$, $P = 0.04$). Although baseline performance IQ had a significantly negative association with baseline SSRT ($r_{324} = -0.16$, $P = 0.004$), we found no significant correlation between baseline performance IQ and ∆SSRT ($r_{324} = -0.08$, $P = 0.13$). In addition, baseline SSRT was significantly correlated with ∆SSRT ($r_{324} = 0.47$, $P = 1.48 \times 10^{-19}$) (Fig. 2C). In this study, we wanted to discover whether certain baseline brain measures could predict the individual development of SSRT, so we controlled the effect of nonbrain information by regressing site information and baseline SSRT out of the ∆SSRT. The ∆SSRT and ∆SSRT residual were both normally distributed (one sample Kolmogorov–Smirnov test, $P = 0.47$ for ∆SSRT and $P = 0.06$ for ∆SSRT residual), and considerable variability existed in both ∆SSRT and ∆SSRT residual (Fig. 2B, D). The residual of the ∆SSRT was used for the subsequent prediction analyses.

Individualized Prediction of SSRT Development Using Baseline Functional Connectivity

We next tested whether the baseline SST-related functional connectivity could predict the individual development of SSRT, i.e., ∆SSRT residual. A functional connectivity matrix was derived by correlating the average time series between each possible pair of ROIs and was then Fisher z-transformed. Here, we restricted our analyses to functional connections between 2 different networks (66 groups) or within 1 network (12 groups), generating 78 groups of functional connectivity features. Each group of functional connectivity features was separately used to predict the ∆SSRT residual.

Of the 78 models predicting the ∆SSRT residual, the model using the functional connections between the ventral attention network (VAN) and the subcortical network gave the optimal prediction performance ($r_{324} = 0.24$, $P = 4 \times 10^{-4}$ using 10 000 permutation tests) (Fig. 3A) and was the only one that survived Bonferroni correction. For this VAN-Subcortical prediction model, the scatter plot of the predicted and observed values is shown in Fig. 3B. The predicted ∆SSRT residual had no site effect (one-way ANOVA, $F_{7,318} = 1.66$, $P = 0.12$) and was not correlated with baseline SSRT ($r_{324} = 0.02$, $P = 0.7$) but was negatively correlated with follow-up SSRT ($r_{324} = -0.21$, $P = 1.01 \times 10^{-4}$).

The prediction results were unlikely to be affected by the fMRI confounding factors (i.e., FD and the number of remaining frames) for 2 reasons. First, the actual ∆SSRT was not significantly correlated with the two factors (FD: $r_{324} = 0.01$, $P = 0.86$, number of frames: $r_{324} = 0.01$, $P = 0.82$). Second, since the predicted ∆SSRT residual by the VAN-Subcortical prediction model was correlated with the baseline FD and the number of

Table 1 Demographic information and SST performance for the 326 participants

	Baseline[a]	Follow-up[a]	Paired t-test (two-tailed)	
			t	P
Age (years)	14.44 (0.42)	19.05 (0.72)	−117.59	0
Gender	Female/male = 187/139		-	-
Handedness	Right/left/both = 289/35/2		-	-
Site	53/42/1/14/68/40/57/51			
Verbal IQ[b]	84 (10)	-	-	-
Performance IQ[b]	111 (13)	-	-	-
pSF	0.5 (0.02)	0.49 (0.02)	1.68	0.09
pGoL	0.009 (0.02)	0.008 (0.02)	0.91	0.36
pGoW	0.05 (0.03)	0.05 (0.03)	−0.85	0.4
Go RT (ms)	422 (59)	373 (52)	15.15	1.3×10^{-39}
RT on SF (ms)	387 (58)	330 (45)	17.43	1.67×10^{-48}
GoS RT (ms)	425 (58)	376 (51)	15.61	2.27×10^{-41}
GoS RT std	98 (23)	81 (23)	11.7	1.22×10^{-26}
SSD (ms)	197 (67)	143 (63)	12.96	2.91×10^{-31}
SSRT (ms)	211 (32)	219 (40)	−3.09	0.002

Note:-, not applicable. pSF, the proportion of Stop Failure in stop trials; pGoL, the proportion of Go Too Late in go trials; pGoW, the proportion of Go Wrong in go trials; Go RT, mean reaction time in go trials (Go Success and Go Wrong trials); RT on SF, mean reaction time in Stop Failure and Stop Too Early trials; GoS RT, mean reaction time in Go Success trials; GoS RT std, standard deviation of reaction time in Go Success trials; SSD, mean stop signal delay; SSRT, stop signal reaction time. [a]Mean (standard deviation). [b]The IQ are raw values without age-normalization.
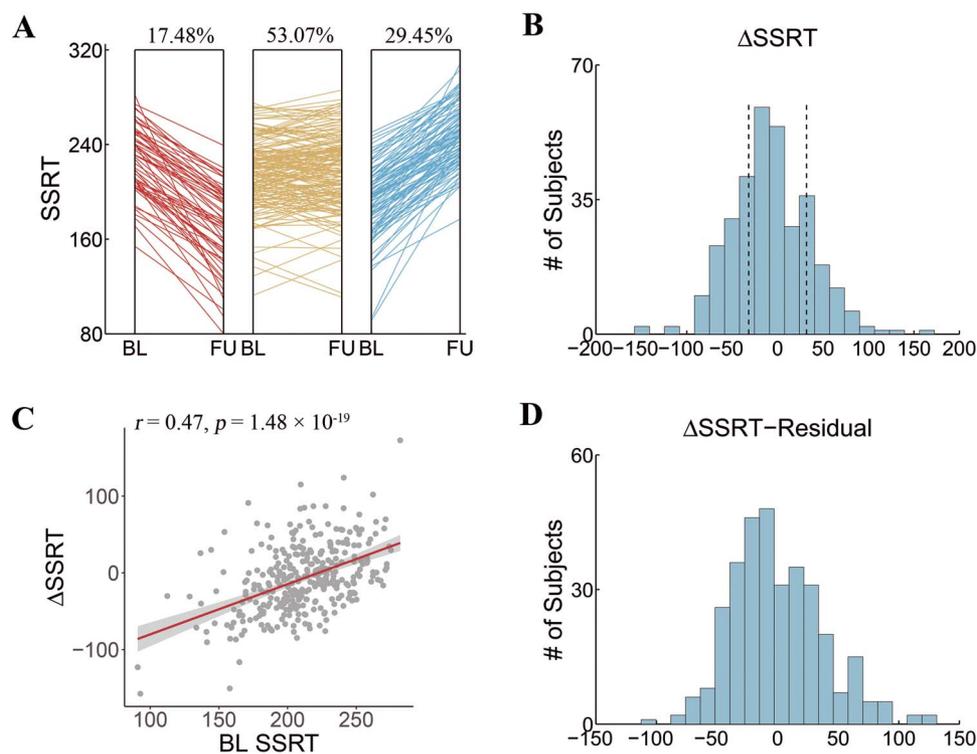
Figure 2. Individual differences in SSRT-measured development (N = 326). (A) SSRT-measured development from age 14 (baseline) to age 19 (follow-up) for each subject. A decreased SSRT indicates an improvement in inhibitory control ability. From left to right, the 3 columns colored in red, yellow, and blue respectively show subjects whose SSRTs decreased (17.48%)/remained stable (53.07%)/increased (29.45%). (B) Histogram representing the distribution of ΔSSRT (baseline SSRT—follow-up SSRT). The dashed lines show the reliable change threshold (± 31.88 ms) in 2 directions. (C) Correlation between the baseline SSRT and ΔSSRT. There was a significantly positive correlation between the baseline SSRT and ΔSSRT ($r_{324} = 0.47$, P = 1.48×10^{-19}). (D) Histogram representing the distribution of ΔSSRT after regressing out site information and the baseline SSRT. The ΔSSRT residual was further predicted using the brain functional connectivity features. BL, baseline; FU, follow-up.

remaining frames (FD: $r_{324} = 0.16$, P = 0.004, number of frames: $r_{324} = -0.13$, P = 0.02), the effects of the 2 factors were ruled out when correlating the predicted and observed outcomes, as mentioned above. We also provided results without regressing

the 2 fMRI confounding factors out (Fig. S2). Since the actual ΔSSRT showed no correlation with the 2 factors, the prediction results with or without regressing out them were quite similar. The VAN-Subcortical prediction model was also the only one
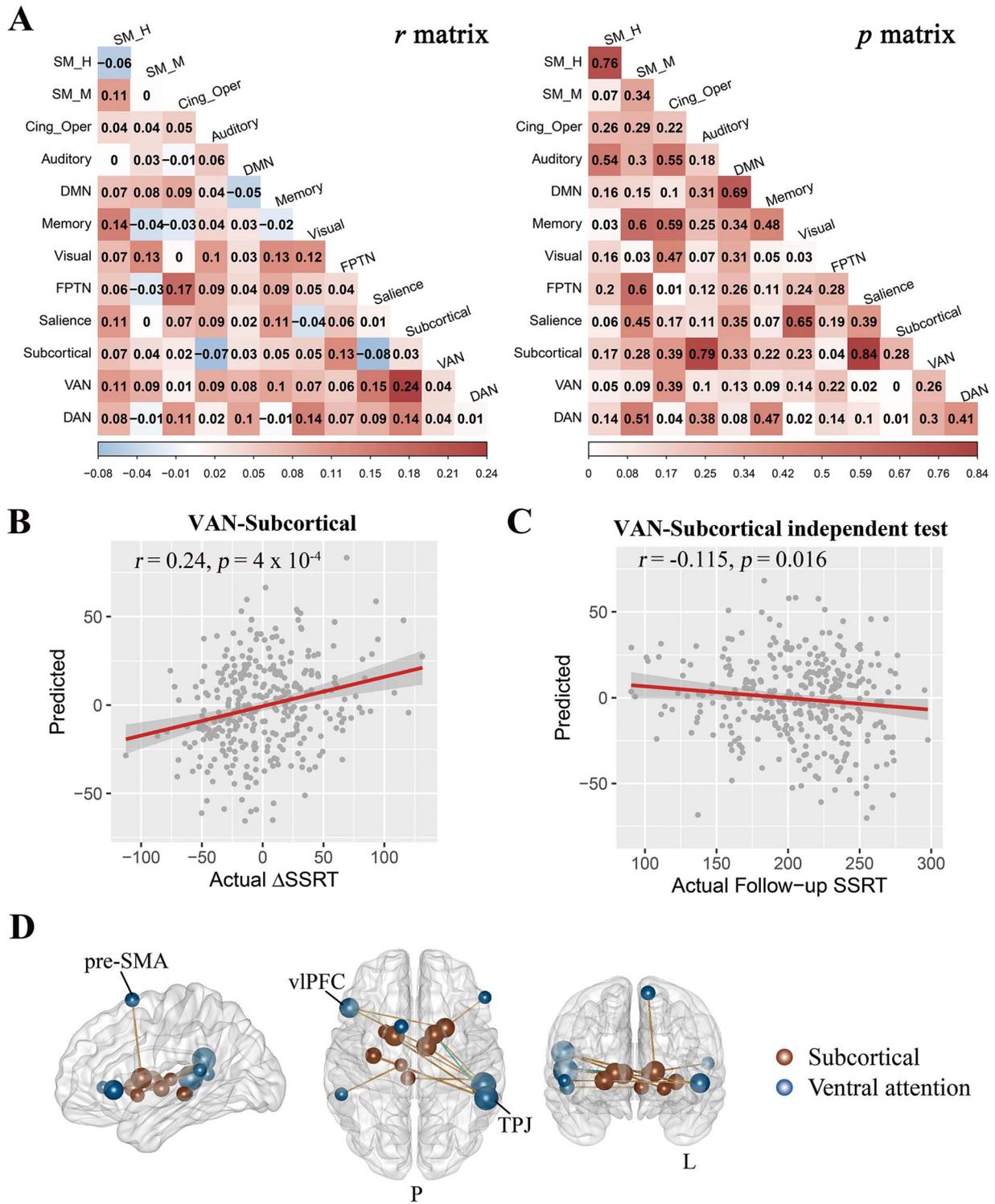
Figure 3. Prediction results of ΔSSRT residual using brain functional connectivity profiles. (A) The prediction performance of each of the 78 models (left panel: r values; right panel: the corresponding P values derived from 10 000 permutations). Only the model using VAN-Subcortical interconnections as features survived Bonferroni correction. (B) The scatter plot of predicted and actual ΔSSRT residual for the VAN-Subcortical prediction model ($r_{324} = 0.24$, $P = 4 \times 10^{-4}$). (C) Independent validation of the VAN-Subcortical prediction model on subjects with baseline fMRI, and follow-up SSRT but without baseline SSRT ($N = 344$). There was a significant negative correlation between the predicted ΔSSRT residual and the actual follow-up SSRT ($r_{342} = -0.115$, $P = 0.016$). (D) Functional connections with significant weights in the VAN-Subcortical prediction model. The brain are shown from the sagittal left (left), axial superior (middle), and coronal anterior (right) views. Brown lines denote positive weights, and blue lines represent negative weights. Nodes in VAN are colored dark blue and nodes in subcortical are colored dark brown. Line width characters the absolute weight of each connection, whereas the size of a node represents the sum of absolute weights of its connections. SM_H, sensory/somatomotor hand; SM_M, sensory/somatomotor mouth; Cing_Oper, cingulo-opercular task control; DMN, default mode; Memory, memory retrieval; FPTN, frontoparietal task control; VAN, ventral attention; DAN, dorsal attention network; Pre-SMA, presupplementary motor area; TPJ, temporoparietal junction; vlPFG, ventral lateral prefrontal gyrus.

that survived Bonferroni correction ($r_{324} = 0.25$, $P = 3 \times 10^{-4}$ using 10 000 permutation tests) when we did not remove the effects of the 2 fMRI confounding factors.

Compared with network-based functional connectivity, whole-brain functional connectivity has the advantage of containing more information but may also introduce useless information that could confound predictions. We further tested whether whole-brain functional connectivity could predict individual development, as measured by the SSRT. To this end, the same prediction process as that used for the network-based prediction was performed, except that we used the 26 796 ($232 \times 231/2$) dimensions of the whole-brain functional connectivity as features. The model utilizing whole-brain functional connectivity as features failed to predict the individual development measured by SSRT ($r_{324} = 0.06$, $P = 0.2$ using 10 000 permutation tests, Fig. S3), which may suggest a relatively localized neural mechanism in IC development.

Reproducibility and Generalizability of the VAN-Subcortical Prediction Model

Given the diversities in choosing the brain atlases for defining ROIs, we tested the reproducibility of the VAN-Subcortical prediction model using a different atlas. Since network definitions vary a lot across studies (Cui et al. 2020), it was not appropriate to replicate our results at the network level. So we directly localized the 9 ROIs in VAN and the 13 ROIs in subcortical network defined by Power (Power et al. 2011) to the ROIs defined by Shen's atlas (Shen et al. 2013), which is also often used to character the relationship between the functional connectivity and cognition abilities (Finn et al. 2015; Rosenberg et al. 2016; Beaty et al. 2018). Then VAN-Subcortical interconnections were calculated based on ROIs found in Shen's atlas, and the same 10-fold CV prediction process using these connections as features was performed. These connections could also predict the individual development of IC ($r_{324} = 0.15$, $P = 0.006$ using 10 000 permutation tests).

In addition, we tested the reproducibility of the VAN-Subcortical prediction model using another 2 connectivity measures (accordance and discordance). The VAN-Subcortical interconnections constructed with accordance and discordance were separately used as features in the 10-fold CV prediction process. For the accordance, the performance of the VAN-Subcortical prediction model was significant in 4 of the 5 q-values ($r_{324} = 0.19$, 0.19, 0.21, 0.13, 0.08; $P = 0.004$, 0.005, 0.002, 0.03, 0.113), with $q = 80$ showing the best performance. For the discordance, the prediction performance was significant in all the 5 q-values ($r_{324} = 0.27$, 0.29, 0.21, 0.17, 0.13; $P = 3 \times 10^{-4}$, $<10^{-4}$, 0.004, 0.011, 0.038), with $q = 75$ showing the best performance.

To test the generalizability of the VAN-Subcortical prediction model, we applied the model to an independent dataset (subjects with baseline fMRI and follow-up SSRT but without baseline SSRT, $N = 344$). Specifically, we built the VAN-Subcortical prediction model using all the 326 subjects in the ΔSSRT residual prediction set. Then we entered the functional connectivity between the VAN and subcortical network for each subject in the test set into the model and got the predicted ΔSSRT residual. None of the demographic information (baseline age, age latency, gender, handedness, site, baseline verbal IQ, and baseline performance IQ) nor the baseline fMRI confounding factors (head motion and the number of remaining frames) affected the predicted score. So, we directly correlated the predicted score with the follow-up SSRT and found a negative correlation

between them ($r_{342} = -0.115$, $P = 0.016$ using 10 000 permutation tests) (Fig. 3C). Here we correlated the predicted values with follow-up SSRTs instead of with ΔSSRTs, as baseline SSRTs were not available for calculating ΔSSRTs in these subjects. The negative correlation was because of the ΔSSRT definition (baseline SSRT—follow-up SSRT).

Contributing Connections and Nodes in the VAN-Subcortical Prediction Model

Permutation test was used to find connections which made significant contributions to the VAN-Subcortical prediction model. Twelve of the 117 (9×13, 9 ROIs in the VAN and 13 ROIs in the subcortical network) connections had significant weights ($P < 0.05$, two-tailed, uncorrected), and they are shown in Figure 3D and Table S3. These 12 connections located in 8 of the 9 ROIs in the VAN, which are anchored in the temporoparietal junction (TPJ), ventral lateral prefrontal cortex (vlPFC), and left premotor and supplementary motor area (pre-SMA); and in 8 of the 13 nodes in the subcortical network, which primarily located in thalamus, pallidum, putamen, and caudate.

Relationship between VAN-Subcortical Functional Connectivity and Follow-Up Substance Abuse

Poor IC has been reported to be relevant to substance abuse during adolescence (Romer Thomsen et al. 2018). So, we next examined whether the functional connectivity found to predict SSRT-related development was further related to follow-up substance abuse (alcohol, nicotine, and illicit drugs). Here, we defined future substance abusers as subjects who were substance nonusers at baseline but turned into substance abusers at follow-up, and the controls as subjects who were substance nonusers at both baseline and follow-up. Pairwise connectivity values between the VAN and subcortical network were summed for each subject at baseline (termed the VAN-Subcortical functional connectivity measure). An ANCOVA was used to compare this baseline VAN-Subcortical functional connectivity measure between the future substance abuse group ($N = 102$) and the control group ($N = 56$) (demographics can be found in Table S4), controlling the effects of demographics, FD and number of remaining frames for the baseline fMRI, as well as baseline lifetime use of substances and time-to-initiation. We found that the baseline VAN-Subcortical functional connectivity measure was significantly higher in future abusers than in the controls ($F_{1,137} = 7.42$, $P = 0.007$) (Fig. 4A). Different values to represent the age of substance use onset for subjects who have not tried any substance did not affect the results. Because the proportion of male future abusers (female/male = 40/62) was significantly larger than that of controls (female/male = 33/23) ($\chi^2 = 5.65$, $P = 0.017$), we further matched the gender by successively removing the male subjects who abused more than one/only one kind of substance in the future abusers. A higher baseline VAN-Subcortical connectivity measure was also found in future abusers when gender was matched ($F_{1,114} = 6.23$, $P = 0.015$; $F_{1,98} = 9.27$, $P = 0.003$, Fig. S4A).

We also separately compared all the 78 groups of within-network and between-network functional connectivity between the future substance abusers and the controls. The results are shown in Figure S5. Among the 78 groups, 7 of them could predict the future substance abuse ($P < 0.05$, uncorrected), with the VAN-Subcortical interconnections ranking third. This illustrated that the brain difference was not a global effect. It should be mentioned that the VAN-Subcortical interconnections did not
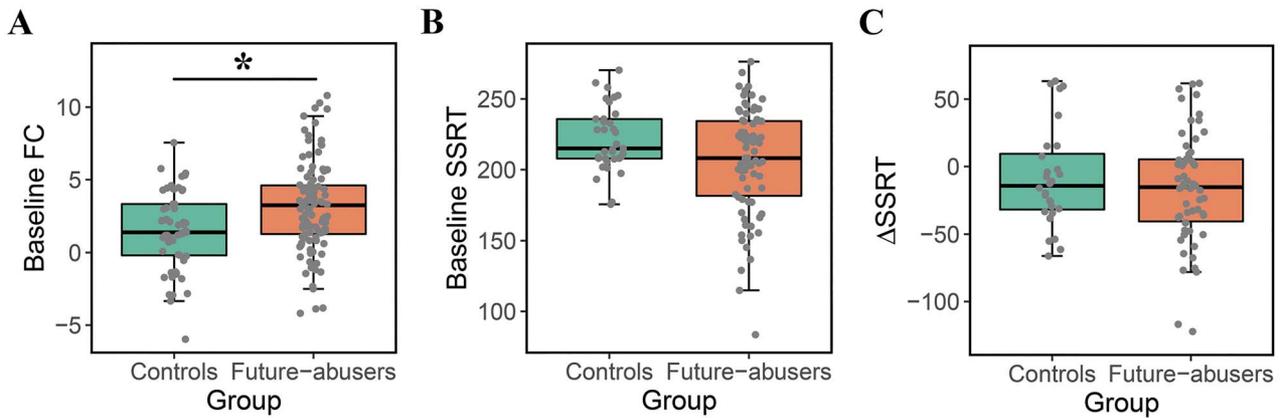
Figure 4. Relationship between inhibitory control and follow-up substance abuse. For the box-and-whisker plots with original data points (dark gray circles), the central line in each box represents the median; the top and bottom edges of the box indicate the 25th and 75th percentiles of the sample; and the whiskers represent $1.5 \times$ the interquartile range. (A) Relationship between the baseline VAN-Subcortical functional connectivity measure and follow-up substance abuse. The baseline VAN-Subcortical functional connectivity measure in future substance abusers ($N = 102$) was significantly higher than that in the controls ($N = 56$) ($F_{1,137} = 7.42$, $P = 0.007$). $*P < 0.05$. (B) Relationship between baseline SSRT and follow-up substance abuse. There was no significant difference in baseline SSRT between the future abuser group ($N = 75$) and the control group ($N = 35$) ($F_{1,91} = 2.87$, $P = 0.1$). (C) Relationship between $\triangle$SSRT and follow-up substance abuse. No difference was found in $\triangle$SSRT between the controls ($N = 28$) and the future abusers ($N = 58$) ($F_{1,67} = 0.15$, $P = 0.7$).

rank first as that in the SSRT development prediction, illustrating both similarities and differences existed in the neural mechanisms between the development of IC and initiation of substance abuse.

In addition to the baseline functional connectivity measures, we examined whether the baseline SSRT or the $\triangle$SSRT was related to follow-up substance abuse by comparing the baseline SSRT or the $\triangle$SSRT between the future abusers and the controls (demographics are shown in Tables S5 and S6). No significant difference was found in both baseline SSRT ($F_{1,91} = 2.87$, $P = 0.1$, Fig. 4B) and $\triangle$SSRT ($F_{1,67} = 0.15$, $P = 0.7$, Fig. 4C) between the 2 groups, which suggests that the change in substance abuse was not associated with baseline SSRT and SSRT-related development. Different values to represent the time of initiation of substance use for subjects who have not experimented any substance also did not affect the results. We also performed an ANCOVA after matching the gender and found similar results in both the baseline SSRT ($F_{1,75} = 2.94$, $P = 0.09$; $F_{1,63} = 3.76$, $P = 0.06$) and the $\triangle$SSRT ($F_{1,57} = 0.1$, $P = 0.76$; $F_{1,46} = 1.06$, $P = 0.32$) (Fig. S4B, C).

Discussion

We studied the individual development of IC in adolescents and tried to identify the early neural predictive biomarkers for the development with longitudinal SST data with a 5-year latency. The developmental trajectory of IC from mid- to late-adolescence differed across subjects. Among all the baseline candidate functional connectivity groups, the VAN and subcortical interconnections could reliably predict the individual development measured by the SSRT, controlling the effects of nuisance covariates and baseline SSRT. The VAN-Subcortical prediction model survived corrections for multiple comparisons and could be generalized to previously unseen subjects to predict their future IC. In addition, the baseline VAN-Subcortical functional connectivity was related to future substance abuse, an IC-deficit related maladaptive behavior. Identifying the early neural predictors for the development of IC and substance abuse

in adolescents may be especially important in that interventions could be expected to be more effective during a period of development with high plasticity.

There are great individual variations in the development of IC from mid- to late-adolescence with some subjects showing IC decrements/increments and others remaining stable. This individual variation can partially explain the discrepant results of group-level analyses on IC development, especially for studies with small sample sizes. Our study further demonstrated the necessity of studying adolescent neurocognitive development while taking into account different developmental trajectories. Also, combined with the previous finding of individual differences in the development of IC from early- to midadolescence (Fosco et al. 2019), we revealed that the development of IC shows great individual variations across the whole span of adolescence.

As for the demographic factors affecting the development of IC, we found that individuals who had a faster IC in midadolescence tended to show an ability decrement in late-adolescence. We also observed that site had an effect on IC development. A possible explanation is that adolescents may show different IC development trajectories in different cities. In contrast, baseline age and age latency showed no effect on IC development in our study, a finding which may have been caused by the homogeneity of the ages that we studied. Unlike studying subjects within a large age band, the homogeneity of age enabled us to analyze the development at a specific age without the need to factor out possible age differences. The development of IC also did not appear to be affected by IQ or gender, findings which are consistent with a previous antisaccade study (Ordaz et al. 2013).

Functional connectivity profiles between the VAN and subcortical network at the baseline could predict individual development of IC over a span of 5 years, even after removing the effect of nuisance covariates and the baseline SSRT. This result was replicated with a different atlas and 2 different functional connectivity metrics. The VAN is anchored in the TPJ, vlPFC, and left pre-SMA, and its key function is to direct attention to stimuli

outside of the current focus (Corbetta et al. 2008). Also, previous studies showed that the VAN is strongly activated during SST (Zhang et al. 2017; Cai et al. 2019). The subcortical network is primarily located in the thalamus, pallidum, putamen, and caudate. Although previous results have shown their role in IC and that their development accompanies IC changes across adolescence, we are unaware of any prior work reporting their ability to predict future IC development.

The neural substrate of inhibition that is currently widely accepted is the frontobasal-ganglia network, a concept which has been supported by different methods including fMRI activation studies (Zhang et al. 2017), brain damage studies in both animals (Eagle and Robbins 2003) and humans (Aron et al. 2003; Rieger et al. 2003), transcranial magnetic stimulation studies (Chambers et al. 2006; Chambers et al. 2007), and others. Specifically, the right IFG and pre-SMA in the frontal lobe appear to work together to send a stop command to the basal ganglia, which then suppresses the thalamocortical programs, thereby blocking the execution of the go response (Verbruggen and Logan 2008; Aron 2011). Additionally, the structure and function of the frontal and striatal regions are not yet well developed by late-adolescence in that they show a significant reduction in gray matter density (Sowell et al. 1999) and changes in activation during motor inhibition from adolescence to young adulthood (Rubia et al. 2006; Braet et al. 2009). Corticostriatal connectivity mediates a wide repertoire of goal-directed behaviors (Marquand et al. 2017), and structural connectivity has been shown to exist between the frontal lobe and striatum (Leh et al. 2007). Furthermore, improved inhibition ability with age was coupled with more restricted diffusion in frontostriatal tracts (Liston et al. 2006) and an increase in frontostriatal functional connectivity (Vink et al. 2014). We speculate that the important role of the frontal lobe, striatum, and connections between them in IC, as well as their immaturity during adolescence, provide a foundation for their ability to predict individual IC development.

It is often difficult to disentangle the cause and effect relationship between brain deficits and substance abuse. Here by using a longitudinal dataset, we found that subjects with higher functional connectivity between the VAN and subcortical network at the baseline tended to become substance abusers within 5 years, which suggests that a functional connectivity difference precedes substance abuse. Similarly, altered frontostriatal white matter microstructure has been shown to be associated with future binge drinking (Jones and Nagel 2019), and abnormal activations in the prefrontal and subcortical regions during an IC-related task have also been found to predict future substance use (Romer Thomsen et al. 2018).

It should be mentioned that we compared the sum of functional connectivity between the VAN and Subcortical rather than the predicted values derived from the VAN-Subcortical prediction model. In fact, by comparing the predicted values of VAN-Subcortical prediction model, we found no significant difference between the future substance abusers and the controls ($F_{1,137} = 1.77$, $P = 0.19$). On the other hand, although the pattern of VAN-Subcortical connectivity could predict the individual development measured by the SSRT, the baseline VAN-Subcortical functional connectivity measure was not significantly correlated with the ΔSSRT ($r_{324} = 0.04$, $P = 0.51$). In addition, although the VAN-Subcortical interconnections ranked first among all groups of within-network or between-network connections in predicting the individual development of IC, it ranked third in predicting future substance abuse. These findings suggest that both similarities and differences exist in the neural mechanisms between SSRT development and the occurrence of substance abuse.

Also, compared with the baseline SSRT and ΔSSRT, the brain functional connectivity features that predicted the IC development were found to be associated with the future IC-deficit related behavioral problem, i.e., substance abuse. This potentially indicated that IC-related brain features were more sensitive than IC-related behavioral data in predicting future substance abuse. Moreover, this is similar to a previous study in which brain features found in predicting sustained attention also predicted the attention-deficit symptoms in attention deficit hyperactivity disorder (Rosenberg et al. 2016). Therefore, if the features that are found to predict a certain trait can be tested on that trait's clinical symptoms, we can validate the models' reliability and also extend the model's function in clinical situations.

In summary, our work found individual differences in the development of IC from mid- to late-adolescence. Functional connectivity between the VAN and subcortical network can reliably predict the individual development of IC. Although the baseline SSRT is correlated with IC development, discovering the early neural predictors for the development can provide a neural basis for early individualized interventions to avoid IC deficits in adolescents. Furthermore, baseline VAN-Subcortical functional connectivity can characterize future substance abuse, indicating a possible pathway for this neural predictor to clinical translation. In addition, adolescence is a transitional developmental period rather than a single snapshot, and the transitions into and out of adolescence are equally important (Casey et al. 2008). Future work that includes multiple longitudinal time points across the whole span of adolescence may help us better understand the development of IC in adolescence.

Supplementary material

Supplementary material can be found at *Cerebral Cortex* online.

Notes

Funding

References

Aite A, Cassotti M, Linzarini A, Osmont A, Houde O, Borst G. 2018. Adolescents' inhibitory control: keep it cool or lose control. *Dev Sci*. 21:e12491.

Akkermans SEA, Luijten M, van Rooij D, Franken IHA, Buitelaar JK. 2018. Putamen functional connectivity during inhibitory control in smokers and non-smokers. *Addict Biol*. 23:359–368.

Aron AR. 2011. From reactive to proactive and selective control: developing a richer model for stopping inappropriate responses. *Biol Psychiatry*. 69:e55–e68.

Aron AR, Fletcher PC, Bullmore ET, Sahakian BJ, Robbins TW. 2003. Stop-signal inhibition disrupted by damage to right inferior frontal gyrus in humans. *Nat Neurosci*. 6:115–116.

Beaty RE, Kenett YN, Christensen AP, Rosenberg MD, Benedek M, Chen Q, Fink A, Qiu J, Kwapil TR, Kane MJ et al. 2018. Robust prediction of individual creative ability from brain functional connectivity. *Proc Natl Acad Sci USA*. 115:1087–1092.

Braet W, Johnson KA, Tobin CT, Acheson R, Bellgrove MA, Robertson IH, Garavan H. 2009. Functional developmental changes underlying response inhibition and error-detection processes. *Neuropsychologia*. 47:3143–3151.

Büchel C, Peters J, Banaschewski T, Bokde AL, Bromberg U, Conrod PJ, Flor H, Papadopoulos D, Garavan H, Gowland P et al. 2017. Blunted ventral striatal responses to anticipated rewards foreshadow problematic drug use in novelty-seeking adolescents. *Nat Commun*. 8:14140.

Cai W, Duberg K, Padmanabhan A, Rehert R, Bradley T, Carrion V, Menon V. 2019. Hyperdirect insula-basal-ganglia pathway and adult-like maturity of global brain responses predict inhibitory control in children. *Nat Commun*. 10:1–13.

Casey BJ. 2015. Beyond simple models of self-control to circuit-based accounts of adolescent behavior. *Annu Rev Psychol*. 66:295–319.

Casey BJ, Jones RM, Hare TA. 2008. The adolescent brain. *Ann N Y Acad Sci*. 1124:111–126.

Chambers CD, Bellgrove MA, Stokes MG, Henderson TR, Garavan H, Robertson IH, Morris AP, Mattingley JB. 2006. Executive "brake failure" following deactivation of human frontal lobe. *J Cogn Neurosci*. 18:444–455.

Chambers CD, Bellgrove MA, Gould IC, English T, Garavan H, McNaught E, Kamke M, Mattingley JB. 2007. Dissociable mechanisms of cognitive control in prefrontal and premotor cortex. *J Neurophysiol*. 98:3638–3647.

Chambers RA, Taylor JR, Potenza MN. 2003. Developmental neurocircuitry of motivation in adolescence: a critical period of addiction vulnerability. *Am J Psychiatry*. 160:1041–1052.

Cohen JR, Asarnow RF, Sabb FW, Bilder RM, Bookheimer SY, Knowlton BJ, Poldrack RA. 2010. Decoding developmental differences and individual variability in response inhibition through predictive analyses across individuals. *Front Hum Neurosci*. 4:47.

Congdon E, Mumford JA, Cohen JR, Galvan A, Canli T, Poldrack RA. 2012. Measurement and reliability of response inhibition. *Front Psychol*. 3:37.

Corbetta M, Patel G, Shulman GL. 2008. The reorienting system of the human brain: from environment to theory of mind. *Neuron*. 58:306–324.

Cui Z, Li H, Xia CH, Larsen B, Adebimpe A, Baum GL, Cieslak M, Gur RE, Gur RC, Moore TM. 2020. Individual variation in functional topography of association networks in youth. *Neuron*. 106:340–353.e8.

Dale AM. 1999. Optimal experimental design for event-related fMRI. *Hum Brain Mapp*. 8:109–114.

Dosenbach NU, Nardos B, Cohen AL, Fair DA, Power JD, Church JA, Nelson SM, Wig GS, Vogel AC, Lessov-Schlaggar CN et al. 2010. Prediction of individual brain maturity using fMRI. *Science*. 329:1358–1361.

Durston S, Thomas KM, Yang Y, Uluğ AM, Zimmerman RD, Casey B. 2002. A neural basis for the development of inhibitory control. *Dev Sci*. 5:F9–F16.

Eagle DM, Robbins TW. 2003. Inhibitory control in rats performing a stop-signal reaction-time task: effects of lesions of the medial striatum and d-amphetamine. *Behav Neurosci*. 117:1302–1317.

Fair DA, Cohen AL, Power JD, Dosenbach NU, Church JA, Miezin FM, Schlaggar BL, Petersen SE. 2009. Functional brain networks develop from a "local to distributed" organization. *PLoS Comput Biol*. 5:e1000381.

Filbey F, Yezhuvath U. 2013. Functional connectivity in inhibitory control networks and severity of cannabis use disorder. *Am J Drug Alcohol Abuse*. 39:382–391.

Finn ES, Shen X, Scheinost D, Rosenberg MD, Huang J, Chun MM, Papademetris X, Constable RT. 2015. Functional connectome

fingerprinting: identifying individuals using patterns of brain connectivity. *Nat Neurosci.* 18:1664–1671.

Fosco WD, Hawk LW Jr, Colder CR, Meisel SN, Lengua LJ. 2019. The development of inhibitory control in adolescence and prospective relations with delinquency. *J Adolesc.* 76:37–47.

Foulkes L, Blakemore SJ. 2018. Studying individual differences in human adolescent brain development. *Nat Neurosci.* 21:315–323.

Gordon EM, Laumann TO, Gilmore AW, Newbold DJ, Greene DJ, Berg JJ, Ortega M, Hoyt-Drazen C, Gratton C, Sun H et al. 2017. Precision functional mapping of individual human brains. *Neuron.* 95:791, e797–807.

Greene AS, Gao S, Scheinost D, Constable RT. 2018. Task-induced brain state manipulation improves prediction of individual traits. *Nat Commun.* 9:2807.

Heatherton TF, Kozlowski LT, Frecker RC, Fagerstrom KO. 1991. The Fagerstrom test for nicotine dependence: a revision of the Fagerstrom tolerance questionnaire. *Br J Addict.* 86:1119–1127.

Hibell B, Andersson B, Bjarnason T, Kokkevi A, Morgan M, Narusk A, Ahlström S 1997. The 1995 ESPAD report: alcohol and other drug use among students in 26 European countries. (Swedish Council for Information on Alcohol and Other Drugs).

Humphrey G, Dumontheil I. 2016. Development of risk-taking, perspective-taking, and inhibitory control during adolescence. *Dev Neuropsychol.* 41:59–76.

Hwang K, Velanova K, Luna B. 2010. Strengthening of top-down frontal cognitive control networks underlying the development of inhibitory control: a functional magnetic resonance imaging effective connectivity study. *J Neurosci.* 30:15535–15545.

Insel TR. 2014. Mental disorders in childhood: shifting the focus from behavioral symptoms to neurodevelopmental trajectories. *JAMA.* 311:1727–1728.

Iverson GL. 2001. Interpreting change on the WAIS-III/WMS-III in clinical samples. *Arch Clin Neuropsychol.* 16:183–191.

Jones SA, Nagel BJ. 2019. Altered frontostriatal white matter microstructure is associated with familial alcoholism and future binge drinking in adolescence. *Neuropsychopharmacology.* 44:1076–1083.

Kaufmann T, Alnaes D, Doan NT, Brandt CL, Andreassen OA, Westlye LT. 2017. Delayed stabilization and individualization in connectome development are related to psychiatric disorders. *Nat Neurosci.* 20:513–515.

Kelley TL. 1925. The applicability of the spearman-Brown formula for the measurement of reliability. *J Educ Psychol.* 16:300.

Leh SE, Ptito A, Chakravarty MM, Strafella AP. 2007. Frontostriatal connections in the human brain: a probabilistic diffusion tractography study. *Neuroscience letters.* 419:113–118.

Liston C, Watts R, Tottenham N, Davidson MC, Niogi S, Ulug AM, Casey BJ. 2006. Frontostriatal microstructure modulates efficient recruitment of cognitive control. *Cereb Cortex.* 16:553–560.

Logan GD, Cowan WB. 1984. On the ability to inhibit thought and action: a theory of an act of control. *Psychol Rev.* 91:295–327.

Luna B, Garver KE, Urban TA, Lazar NA, Sweeney JA. 2004. Maturation of cognitive processes from late childhood to adulthood. *Child Dev.* 75:1357–1372.

Marquand AF, Haak KV, Beckmann CF. 2017. Functional corticostriatal connection topographies predict goal directed behaviour in humans. *Nat Hum Behav.* 1:1–9.

Meskaldji D-E, Morgenthaler S, Van De Ville D 2015. New measures of brain functional connectivity by temporal analysis of extreme events. In: *2015 IEEE 12th International Symposium on Biomedical Imaging (ISBI)*, pp. 26–29: IEEE.

O'Shea M, Singh ME, McGregor IS, Mallet PE. 2004. Chronic cannabinoid exposure produces lasting memory impairment and increased anxiety in adolescent but not adult rats. *J Psychopharmacol.* 18:502–508.

Ordaz SJ, Foran W, Velanova K, Luna B. 2013. Longitudinal growth curves of brain function underlying inhibitory control through adolescence. *J Neurosci.* 33:18109–18124.

Paulsen DJ, Hallquist MN, Geier CF, Luna B. 2015. Effects of incentives, age, and behavior on brain activation during inhibitory control: a longitudinal fMRI study. *Dev Cogn Neurosci.* 11:105–115.

Paus T, Keshavan M, Giedd JN. 2008. Why do many psychiatric disorders emerge during adolescence? *Nat Rev Neurosci.* 9:947–957.

Plitt M, Barnes KA, Wallace GL, Kenworthy L, Martin A. 2015. Resting-state functional connectivity predicts longitudinal change in autistic traits and adaptive functioning in autism. *Proc Natl Acad Sci USA.* 112:E6699–E6706.

Power JD, Barnes KA, Snyder AZ, Schlaggar BL, Petersen SE. 2012. Spurious but systematic correlations in functional connectivity MRI networks arise from subject motion. *Neuroimage.* 59:2142–2154.

Power JD, Cohen AL, Nelson SM, Wig GS, Barnes KA, Church JA, Vogel AC, Laumann TO, Miezin FM, Schlaggar BL et al. 2011. Functional network organization of the human brain. *Neuron.* 72:665–678.

Rieger M, Gauggel S, Burmeister K. 2003. Inhibition of ongoing responses following frontal, nonfrontal, and basal ganglia lesions. *Neuropsychology.* 17:272–282.

Romer Thomsen K, Blom Osterland T, Hesse M, Feldstein Ewing SW. 2018. The intersection between response inhibition and substance use among adolescents. *Addict Behav.* 78: 228–230.

Rosenberg MD, Casey BJ, Holmes AJ. 2018. Prediction complements explanation in understanding the developing brain. *Nat Commun.* 9:1–13.

Rosenberg MD, Finn ES, Scheinost D, Papademetris X, Shen X, Constable RT, Chun MM. 2016. A neuromarker of sustained attention from whole-brain functional connectivity. *Nat Neurosci.* 19:165–171.

Rubia K, Smith AB, Taylor E, Brammer M. 2007. Linear age-correlated functional development of right inferior fronto-striato-cerebellar networks during response inhibition and anterior cingulate during error-related processes. *Hum Brain Mapp.* 28:1163–1177.

Rubia K, Smith AB, Woolley J, Nosarti C, Heyman I, Taylor E, Brammer M. 2006. Progressive increase of frontostriatal brain activation from childhood to adulthood during event-related tasks of cognitive control. *Hum Brain Mapp.* 27:973–993.

Saunders JB, Aasland OG, Babor TF, de la Fuente JR, Grant M. 1993. Development of the alcohol use disorders identification test (AUDIT): WHO collaborative project on early detection of persons with harmful alcohol consumption–II. *Addiction.* 88:791–804.

Schachar R, Logan GD. 1990. Impulsivity and inhibitory control in normal development and childhood psychopathology. *Dev Psycho.* 26:710–720.

Schumann G, Loth E, Banaschewski T, Barbot A, Barker G, Büchel C, Conrod P, Dalley J, Flor H, Gallinat J et al. 2010. The IMAGEN study: reinforcement-related behaviour in normal brain function and psychopathology. *Mol Psychiatry.* 15:1128–1139.

Shen X, Tokoglu F, Papademetris X, Constable RT. 2013. Groupwise whole-brain parcellation from resting-state fMRI data for network node identification. *Neuroimage*. 82: 403–415.

Sinha R, Easton C, Kemp K. 2003. Substance abuse treatment characteristics of probation-referred young adults in a community-based outpatient program. *Am J Drug Alcohol Abuse*. 29:585–597.

Sowell ER, Thompson PM, Holmes CJ, Jernigan TL, Toga AW. 1999. In vivo evidence for post-adolescent brain maturation in frontal and striatal regions. *Nat Neurosci*. 2:859–861.

Steinberg L, Icenogle G, Shulman EP, Breiner K, Chein J, Bacchini D, Chang L, Chaudhary N, Giunta LD, Dodge KA et al. 2018. Around the world, adolescence is a time of heightened sensation seeking and immature self-regulation. *Dev Sci*. 21:e12532.

Tsvetanov KA, Ye Z, Hughes L, Samu D, Treder MS, Wolpe N, Tyler LK, Rowe JB. 2018. Activity and connectivity differences underlying inhibitory control across the adult life span. *J Neurosci*. 38:7887–7900.

Velanova K, Wheeler ME, Luna B. 2008. Maturational changes in anterior cingulate and frontoparietal recruitment support the development of error processing and inhibitory control. *Cereb Cortex*. 18:2505–2522.

Verbruggen F, Logan GD. 2008. Response inhibition in the stop-signal paradigm. *Trends Cogn Sci*. 12:418–424.

Verbruggen F, Chambers CD, Logan GD. 2013. Fictitious inhibitory differences: how skewness and slowing distort the estimation of stopping latencies. *Psychol Sci*. 24:352–362.

Verbruggen F, Aron AR, Band GP, Beste C, Bissett PG, Brockett AT, Brown JW, Chamberlain SR, Chambers CD, Colonius H et al. 2019. A consensus guide to capturing the ability to inhibit actions and impulsive behaviors in the stop-signal task. *eLife*. 8:e46323..

Vink M, Zandbelt BB, Gladwin T, Hillegers M, Hoogendam JM, van den Wildenberg WP, Du Plessis S, Kahn RS. 2014. Frontostriatal activity and connectivity increase during proactive inhibition across adolescence and early adulthood. *Hum Brain Mapp*. 35:4415–4427.

Whelan R, Conrod PJ, Poline J-B, Lourdusamy A, Banaschewski T, Barker GJ, Bellgrove MA, Büchel C, Byrne M, Cummins TD et al. 2012. Adolescent impulsivity phenotypes characterized by distinct brain networks. *Nat Neurosci*. 15:920–925.

White TP, Loth E, Rubia K, Krabbendam L, Whelan R, Banaschewski T, Barker GJ, Bokde AL, Büchel C, Conrod P et al. 2014. Sex differences in COMT polymorphism effects on prefrontal inhibitory control in adolescence. *Neuropsychopharmacology*. 39:2560–2569.

Williams BR, Ponesse JS, Schachar RJ, Logan GD, Tannock R. 1999. Development of inhibitory control across the life span. *Dev Psychol*. 35:205–213.

Yamashita M, Yoshihara Y, Hashimoto R, Yahata N, Ichikawa N, Sakai Y, Yamada T, Matsukawa N, Okada G, Tanaka SC. 2018. A prediction model of working memory across health and psychiatric disease using whole-brain functional connectivity. *eLife*. 7:e38844.

Yoo K, Rosenberg MD, Hsu WT, Zhang S, Li CR, Scheinost D, Constable RT, Chun MM. 2017. Connectome-based predictive modeling of attention: comparing different functional connectivity features and prediction methods across datasets. *Neuroimage*. 167:11–22.

Zahra D, Hedge C. 2010. The reliable change index: why isn't it more popular in academic psychology. *PsyPAG Quarterly*. 76:14–19.

Zhang R, Geng X, Lee TMC. 2017. Large-scale functional neural network correlates of response inhibition: an fMRI meta-analysis. *Brain Struct Funct*. 222:3973–3990.